

This is a provisional PDF only. Copyedited and fully formatted version will be made available soon.



**ISSN:** 0015-5659

**e-ISSN:** 1644-3284

## **Topographical anatomy of the left ventricular summit: implications for invasive procedures**

**Authors:** Marcin Kuniewicz, Maciej Krupiński, Małgorzata Urbańczyk-Zawadzka, Mateusz K. Hołda, Ravin Defonseka, Tanvi Wadhwa, Nicole Cholewa, Aleksandra Matuszyk, Jerzy Walocha, Halina Dobrzynski

**DOI:** 10.5603/FM.a2022.0096

**Article type:** Original article

**Submitted:** 2022-09-07

**Accepted:** 2022-10-31

**Published online:** 2022-11-28

This article has been peer reviewed and published immediately upon acceptance. It is an open access article, which means that it can be downloaded, printed, and distributed freely, provided the work is properly cited. Articles in "Folia Morphologica" are listed in PubMed.

## **Topographical anatomy of the left ventricular summit: implications for invasive procedures**

Marcin Kuniewicz et al., Anatomy of the left ventricular summit

Marcin Kuniewicz<sup>1,2</sup>, Maciej Krupiński<sup>3</sup>, Małgorzata Urbańczyk-Zawadzka<sup>3</sup>, Mateusz K. Hołda<sup>4,5</sup>, Ravin DeFonseka<sup>1</sup>, Tanvi Wadhwa<sup>1</sup>, Nicole Cholewa<sup>1</sup>, Aleksandra Matuszyk<sup>1</sup>, Jerzy Walocha<sup>1</sup>, Halina Dobrzynski<sup>1,5</sup>

<sup>1</sup>Department of Anatomy, Jagiellonian University Medical College, Krakow, Poland

<sup>2</sup>Department of Electrophysiology, Institute of Cardiology, John Paul II Hospital, Jagiellonian University Medical College, Krakow, Poland

<sup>3</sup>Department of Radiology and Diagnostic Imaging, John Paul II Hospital, Krakow, Poland

<sup>4</sup>HEART - Heart Embryology and Anatomy Research Team, Department of Anatomy, Jagiellonian University Medical College, Poland

<sup>5</sup>Division of Cardiovascular Sciences, The University of Manchester, United Kingdom

Address for correspondence: Marcin Kuniewicz, MD, PhD, Department of Anatomy, Jagiellonian University Medical College, ul. Kopernika 12, 31-034 Kraków, Poland, tel: +48124229511, e-mail:kuniewicz@m@gmail.com

ORCID: 0000-0002-0029-5553

### **ABSTRACT**

**Background:** Recent clinical reports have emphasized the clinical significance of the left ventricular summit (LVS), a specific triangular epicardial area, as the source of ventricular arrhythmias where radiofrequency ablation is of great difficulty.

**Materials and methods:** The macroscopic morphology of the LVS has been assessed in 80 autopsied and 48 angio-CT human hearts. According to Yamada's equation, the size was calculated based on the distance to the first, most prominent septal perforator.

**Results:** The size of the LVS varies from 33.69 to 792.2 mm<sup>2</sup>, is highly variable, and does not correlate with BMI, sex, or age in general. The mean size of the LVS was 287.38 ± 144.95mm<sup>2</sup> in autopsied and angio-CT (p=0.44). LVS is mostly disproportionately bisected by cardiac coronary veins to superior – inaccessible and inferior–accessible areas. The superior aspect dominates over the inferior in both groups (p=0.04). The relation between superior and

inferior groups determines three possible arrangements: the most common type is superior domination (50.2%), then inferior domination (26.6%), and finally, equal distribution (17.2%). In 10.9 %, the inferior aspect is absent. Only 16.4% of the LVS were empty, without additional trespassing coronary arteries.

**Conclusions:** The difference in size and content of the LVS is significant, with no correlation to any variable. The size depends on the anatomy of the most prominent septal perforator artery. The superior, inaccessible aspect dominates, and the LVS is seldom free from additional coronary vessels, thus making this region hazardous for electrophysiological procedures.

**Key words:** left ventricular summit, septal summit, ventricular arrhythmias

## INTRODUCTION

The left ventricular summit (LVS) is a triangular area located at the base of the left ventricle, at the most superior portion of the left epicardial ventricular region. It comprises the apex, septal margin, mitral margin, and base [15,17,27]. Enclosed in the left coronary artery bifurcation was firstly described by McAlpine in 1975 [21] and thirty-five years later revisited by Yamada because of the arrhythmic importance [14,33]. Because of its location, this heart region is complex to approach for electrophysiology procedures, which is why it is also known as the Bermuda triangle [1]. The great cardiac vein divides the LVS into a superior area (named the inaccessible area) and an inferior area (named the accessible area) [20,30] (Figure 1A,C). Epicardially, the LVS is overlapped by the left atrial appendage covering more than 50% of the LVS area (Figure 1B, D) [16,18,25].

There are various approaches to reaching arrhythmias arising from the LVS, but precise targeting of the arrhythmia source may be troublesome [4,6]. Extensive epicardial area and delicate anatomical structures may complicate these approaches [33]. A detailed understanding of the anatomical structure of the LVS and surrounding structures may help in planning and performing ablation procedures within this area. Therefore, this study aimed to analyze morphometrically the cadaveric heart specimens and angio-computed tomography images to provide a more detailed description of the LVS region.

## MATERIALS AND METHODS

This study was approved by the Bioethical Committee of Jagiellonian University (1072.6120.131.2018) and the Hospital Scientific Board approval (NB.060.1.015.2021). The

study protocol conformed to the ethical guidelines of the 1975 Declaration of Helsinki. The methods were carried out in accordance with the approved guidelines.

### ***Study population***

We examined 128 human hearts (88 male and 40 female) in two methods: autopsy and angio-CT examination.

The first method analyzed 80 randomly selected human cadaveric hearts (68 male and 12 female) dissected from donors who died of noncardiac causes. The organs were collected during routine forensic medical autopsies. All hearts were dissected from adults who were on average  $44.4 \pm 15.5$  years old. The average body mass index (BMI) was  $26.1 \text{ kg/m}^2$ , and the mean heart weight was  $442.0 \pm 91.2 \text{ g}$ . The leading causes of death of the studied subjects were suicide, murder, and traffic/home accidents. Donors with known severe anatomic defects, past cardiac surgeries/interventions, or vascular or cardiac pathologies discovered during the autopsy were excluded from this study.

Additionally, contrast-enhanced ECG-gated cardiac computed tomography scans from randomly selected 48 patients (20 male and 28 female) were evaluated. Cardiac computed tomography scans were performed for various clinical reasons in patients who were on average  $57.9 \pm 11.6$  years old and with an average BMI of  $28.1 \text{ kg/m}^2$ . Only patients with no severe anatomic heart defects and no past cardiac surgeries/interventions were included.

### ***Cadaveric dissections***

Hearts were dissected routinely and then placed in 10% paraformaldehyde solution for two months until further observations. Next, the anterior surface of the LVS was exposed by uplifting the left atrial appendage (Figure 2D,E). The left coronary artery was open from the ostium to bifurcation and along the left anterior descending artery (LAD) to expose the septal perforators. The coronary sinus was cannulated with a hemodynamic guidewire, and the great cardiac/anterior interventricular cardiac vein was revealed from the epicardial adipose tissue. Then, measurements were collected with hearts held in their anatomical position using 0.03-mm precision electronic calipers (YATO, YT-7201, Poland).

### ***Cardiac computed tomography protocol***

The *computed tomography* examinations were performed using a 64-row dual-source scanner (Somatom Definition, Siemens, Erlangen, Germany). The contrast-enhanced acquisitions were performed during inspiratory breath hold with the collimation of 0.75mm.



An iodinated contrast agent was injected with an injection rate of 5ml/s [18]. Images were reconstructed with an image matrix of 512 x 512 pixels. The post-processing and study evaluation was performed using a dedicated workstation (Syngovia, Siemens, Erlangen, Germany). Analyses of coronary vessel course over the left ventricle were done by volume rendered reconstructions as well as sagittal, coronal, and transverse presentations. Virtual calipers were used to measure dimensions.

### ***Observations and measurements***

First, the left coronary artery bifurcation pattern was noted, and the angle of bifurcation was measured. Next, the course of the great cardiac/anterior interventricular cardiac vein was studied. The first dominant septal perforator was chosen to encircle the LVS area. The septal margin, mitral margin, and base were established. The following distances were measured: distance from the left coronary artery ostium to bifurcation and distance from bifurcation to the first dominant septal perforator (LVS margin) (Figure 1C). Yamada's equation was used to calculate the LVS surface area by multiplying the bifurcation angle and distance to the septal perforator [18, 33]. Next, the surface area of the LVS superior region (named the inaccessible area) and an inferior region (named the accessible area) were calculated using Sketchandcalc© (iCalc Inc) computer software after precise calibration.

### ***Statistical analysis***

The results are presented as mean values with corresponding standard deviations or percentages. The Shapiro–Wilk test was used to determine if the quantitative data were normally distributed, and Levene's test was performed to verify a relative homogeneity of variance. A Chi-square test was used to evaluate the difference in dichotomous data. The t-test or Mann-Whitney was used to evaluate the differences in diameters, angles, and volumes between study groups. Statistical analyses were conducted using STATISTICA v13.3 software for Windows (StatSoft Inc., Tulsa, OK, USA). Results were considered statistically significant when the p-value was less than 0.05.

## **RESULTS**

The mean size of the LVS combined in cadaveric and CT reached  $287.38\text{mm}^2 \pm 144.95$ . For autopsied hearts  $270.46 \pm 160.21\text{mm}^2$  (33.69 – 792.2 mm<sup>2</sup>), for CT  $291.58\text{mm}^2 \pm 115.5$  Table 1. No statistical differentiation was found between both study groups ( $p=0.44$ ). The superior aspect of the LVS, with  $145.62 \pm 84.35\text{mm}^2$  (6.74-429.12mm<sup>2</sup>), outperforms the

inferior aspect,  $121.69\text{mm}^2 \pm 94.38$  ( $8.96 - 431.13\text{mm}^2$ ). In 13 hearts, 6 (7.5%) cadaveric and 7 (14.6%) CT, there was no inferior aspect (Figure 2D). Statistically, the superior aspect is notably more extensive than the inferior ( $p=0.04$ ); however, no difference was found between both study groups ( $p=0.18$  for the superior and  $p=0.35$  for the inferior aspect).

Analyzing the LVS size to gender – the female summit size of  $244.71\text{mm}^2 \pm 119.92$  was significantly smaller than the male  $293.68\text{mm}^2 \pm 152.3$  ( $p=0.05$ ). Also, in the female subgroup, the inferior aspect is significantly smaller than in the male ( $p<0.01$ ), while no difference was found between superior aspects to the male gender ( $p=0.07$ ). Providing a Pearson coefficient, we have found a mailed correlation of the LVS calculations to BMI in the female group ( $r=0.32$ ,  $p=0.18$ ), while in men, not ( $r=0.03$   $p=0.92$ ). Detailed data are shown in table 2.

Analyzing a combination of the superior to inferior aspects, we determined three main types of LVS. With superior aspect domination, equal distribution, and inferior aspect domination. We established no more than 10% of the difference between the areas as equal distribution. The most common pattern of the LVS (50.2%) is the dominance of the superior aspect (Figure 2A, D). In 26.6% of the hearts, the inferior aspect dominates (Figure 2C, F), while in 17.2% of the hearts, the superior and inferior aspects are equipoise (Figure 2B, E). Analyzing the subgroups, the distribution between studies and genders was similar.

The second exciting observation was coronary vessel distribution inside LVS. Only 21 (16.4%) hearts were out of additional coronary branches. Majority of summits contain at least one (51%), two (32%) to 3 (17%) additional vessels trespassing LVS. We found almost equal distribution from the LAD and circumflex branch of the left coronary artery. In 30 hearts (23.4%), the LVS contains ramus intermedius exiting directly from the trunk of the left coronary artery. More often, female LVS were freer from additional coronary artery branches than males ( $p=0.02$ ) Table 2.

The venous distribution draining into GCV-AIV from the inferior aspect, known as anterior cardiac veins, and tiny veins draining into the right atrium from the superior was not analyzed because of lack of visualization in the CT. In 17 (21.3%) cadaveric hearts, we noticed the conus vein connecting the great cardiac vein and the right atrium below the trunk of the left coronary artery.

The LAA over LVS has been morphologically assessed based on a new simplified shape-based classification [11,28]. The morphology in cadaveric/CT samples was cauliflower 28/16 (34.4%), then chicken wing 23/18 (32%), and arrowhead 29/14 (33.6%) with no statistical difference in distribution. The average distance between the LAA to the LVS

surface was  $5.45 \pm 2.51$  mm, in subgroups  $6.3 \pm 2.55$  mm (2.8-12.2 mm) for cadaveric and  $5.14 \pm 2.47$  mm (1.4–10 mm) for CT samples (Figure 2F). The distance difference between methods was statistically significant ( $p=0.04$ ). Notably, the distance in the female group was greater, reaching  $5.92 \pm 2.6$  mm vs.  $5.11 \pm 2.04$  mm in male hearts ( $p=0.05$ ).

Interestingly almost all measurements of the LVS from cadaveric dissections are not statistically different from those from angio-CT (Table 1). However, the differences in the vessel's calculations differ in both methods. The mean length of the main trunk of the left coronary artery in the cadaveric heart was  $9.02$  mm  $\pm$   $4.04$  and is shorter than the CT control group  $10.54$  mm  $\pm$   $4.18$  ( $p=0.05$ ). Same with the septal perforator,  $18.2$  mm  $\pm$   $5.55$  vs.  $20.06$  mm  $\pm$   $4.47$  ( $p=0.05$ ).

## DISCUSSION

The LVS is not a relatively small region, reminding a minefield because of its content. In this study, we conducted two approaches for a macroscopic morphology assessment of the LVS using cadaveric hearts and CT images of the beating hearts. The general anatomy of LVS is established; nevertheless, precise measurements and calculations have not been provided yet. The size of the LVS varies from  $33.69$  to  $792.2$  mm<sup>2</sup> and does not correlate with BMI, sex, or age in general, however, a mild correlation with BMI was noticed in the female group ( $r=0.32$ ,  $p=0.18$ ). Its size depends on the random exit of the first dominant septal perforator and the angle of bifurcation of the left coronary artery [13,21,33].

The LVS, divided by a great cardiac vein, comprises superior and inferior aspects. In 10.9%, an unusual combination of the septal perforator exit with the course of GCV-AIV may abolish an inferior aspect (figure 2D). Other almost 90% of the LVS are arranged into three patterns. With Superior aspect domination at 50.2%, inferior aspect domination at 26.6%, and equal distribution of aspects at 17.2%. The inferior aspect is significantly smaller than the superior ( $p=0.01$ ). In the female subgroup, the difference between areas is even more significant ( $p<0.001$ ).

The content of the LVS with additional coronary branches (diagonal or marginal) trespassing through is also variable. Only 11% (cadaveric) and 25% (CT) of the LVS were without additional accessory coronary arteries. The percentage of blank LVS is higher in the female group ( $p=0.02$ ), reaching almost 30% possibly, because of smaller area defined. The distribution of trespassing coronary vessels is equal from the left anterior descending and circumflex branch from the left coronary artery. More than 50% of the LVS contain at least one additional coronary artery, while 17% contain three branches, thus making this region

hazardous for potential arterial dissection during epicardial or intravenous cardiology procedures.

From this perspective, coronarography is inevitable before arrhythmia abolishing [29]. The venous system intersects coronary vessels more often deeply than superficially in a  $\frac{3}{4}$  to  $\frac{1}{4}$  ratio, respectively (Figure 1A,D). The relationships between the GCV-AIV and the coronary arteries in the LVS region were noticed before [5,8,20,30].

An interesting observation was found in counting branches exiting from the LAD. More first diagonal branches were found during cadaveric dissections than in CT image analysis ( $p=0.03$ ). Counting arterial branches from open, dissected LAD in cadaveric hearts is far more precise than angio-CT acquisition.

Because the LVS is not a small structure and may reach almost  $8\text{cm}^2$ , a precise electro-anatomical mapping is necessary where ventricular arrhythmia has the earliest activation [2, 3]. The transcatheter approach is limited by transmural mapping via ventricular outflow tracts, pulmonary trunk, aorta, or coronary sinus. That is why the LVS located between them is known as the Bermuda triangle [1]. The epicardial approach (through the pericardial sac) allows mapping only inferior – accessible areas. Recently proposed access via the left atrial appendage is promising; however, on average, only half of the LVS is covered by this structure [15,16]. Another critical issue is that variability of morphology and distance between the LAA, and the surface of the LVS (1.5 – 12.5mm) may impede successful arrhythmia localization and annihilation [24]. In this study, the most common type of left atrial appendage overlapping the LVS was Arrowhead (33.6%), followed by cauliflower (33.4%) and ChickenWing (32%), with almost equal distribution without statistical significance between the type of the study.

### **Implication for electrophysiology procedures**

The ventricular arrhythmias arising from the LVS apex or septal summit are capable from the left coronary cusp (LCC) (Figure 3A red arrows) of the aortic valve or right-left inter leaflet triangle (R-L ILT) (Figure 3A yellow arrow) [4,17,19]. The lower septal summit arrhythmias or located on the right aspect of the LVS are reachable from the right ventricular outflow tract (RVOT), the right coronary cusp of the pulmonic valve (PV), pulmonary trunk (PT), or even pulmonary artery (PA) (Figure 3A light blue arrow) [14]. The left margin is accessible from LAA (figure 3A white arrows) or coronary venous system (figure 3A dark blue arrow) [16,31,32]. A central aspect of the LVS is attainable from the venous system or LAA [11,12,16,18,22]. Hence the possible approach from the venous system (via a great

cardiac vein) might be promising but also challenging because of the cardiac venous system's complex anatomy [5,10,23].

Arrhythmias located in the LVS need to be mapped from a different approach. Once the location is established, the most adjacent structure must be used for RF application. If necessary, a bipolar with double RF applicators should be on the course of the arrhythmia.

Approach from the endocardial region of the left ventricle is impossible because of the heart muscle thickness (Figure 3B) unless using a bipolar RFCA [7].

The direct approach to the LVS provides access through the pericardial sac (figure 3A orange arrows) and may abolish only arrhythmias located in the inferior aspect of the LVS. A critical remark is that access to the pericardial sac with a substernal approach is possible only among patients without previous open chest surgery [9,26].

### **Limitations of the study**

The first limitation was the difference in methods used to compare the size of the LVS. Beating hearts in a biological environment have different spaces between the LAA and the surface of the ventricle. The thickness of the epicardial adipose tissue and the heart muscle also in post-mortem studies were greater.

Choosing the proper septal perforator in a post-mortem study was troublesome. While in the CT study, the perforator looks like a single vessel, in cadaveric sections, we observe not one but two or even three septal perforators at a close distance (Figure 2D). We acknowledge that the most apparent size will set the inferior border of the LVS. The same problem was with depicting diagonal branches in cadaveric specimens. We found statistically more branches in the post-mortem study than in the angio-CT images. We acknowledge that the angio-CT acquisition can depict the minimum 1mm size vessels, smaller septal perforators visible in cadaveric samples, and small additional coronary branches may differ in the calculations.

### **CONCLUSIONS**

This study provided a comprehensive anatomical description of the LVS region. The rapid development of RFCA ablation procedures requires a better understanding of access, distance, diameter, and potential risks of the LVS to terminate arrhythmias. We found that the LVS region is a highly variable anatomical structure. We claim that the most dominant septal perforator in the proximal aspect of LAD (comparing the CT hearts and postmortem) should represent the LVS definition. The LVS is seldom an empty structure and in 90% of the hearts

investigated consists of additional coronary vessels with a variable origin. Therefore, each ablation procedure in this region should have a coronarography before RFCA ablation.

**Conflict of interest:** None declared

## REFERENCES

1. Altmann DR, Knecht S, Sticherling C, et al. Ventricular tachycardia originating from the “Bermuda Triangle”. *Cardiovascular Medicine*. 2013; 16(7–8): 208–210.
2. Anderson RH, Boyett MR, Dobrzynski H, et al. The anatomy of the conduction system: implications for the clinical cardiologist. *J Cardiovasc Transl Res*. 2013; Apr;6(2):187-96. doi: 10.1007/s12265-012-9433-0. Epub 2012 Dec 15. PMID: 23242580.
3. Daniels DV, Lu YY, Morton JB, et al. Idiopathic epicardial left ventricular tachycardia originating remote from the sinus of Valsalva: electrophysiological characteristics, catheter ablation, and identification from the 12-lead electrocardiogram. *Circulation*. 2006; Apr 4;113(13):1659-66. doi: 10.1161/CIRCULATIONAHA.105.611640. Epub 2006 Mar 27. PMID: 16567566.
4. Enriquez A, Malavassi F, Saenz L. et al. How to map and ablate left ventricular summit arrhythmias. *Heart Rhythm*. 2017; 14 (1), 141–148.
5. Gach-Kuniewicz B, Goncerz G, Ali D, et al. Variations of coronary sinus tributaries among patients undergoing cardiac resynchronization therapy. *Folia Morphol (Warsz)*. 2022; May 24. doi: 10.5603/FM.a2022.0044. Epub ahead of print. PMID: 35607878.
6. Hayashi T, Santangeli P, Pathak RK, et al. Outcomes of Catheter Ablation of Idiopathic Outflow Tract Ventricular Arrhythmias With an R Wave Pattern Break in Lead V2: A Distinct Clinical Entity. *Journal of Cardiovascular Electrophysiology*. 2017; 28 (5), 504–514.
7. Igarashi M, Nogami A, Fukamizu S, et al. Acute and long-term results of bipolar radiofrequency catheter ablation of refractory ventricular arrhythmias of deep intramural origin. *Heart Rhythm*. 2020; Sep;17(9):1500-1507.
8. Ishizawa A, Fumon M, Zhou M, et al. Intersection patterns of human coronary veins and arteries. *Anatomical Science International*. 2008; 83 (1), 26–30.
9. Aly I, Rizvi A, Roberts W, et al. Cardiac ultrasound: An Anatomical and Clinical Review. *Translational Research in Anatomy*. 2020; 100083, ISSN 2214-854X,
10. Ito S, Tada H, Naito S, et al. Development and validation of an ECG algorithm for identifying the optimal ablation site for idiopathic ventricular outflow tract tachycardia. *J Cardiovasc Electrophysiol*. 2003; Dec;14(12):1280-6.
11. Kimura T, Takatsuki S, Inagawa K, et al. Anatomical characteristics of the left atrial appendage in cardiogenic stroke with low CHADS2 scores. *Heart Rhythm* 2013; 10:921–925.
12. Komatsu Y, Nogami A, Shinoda Y, et al. Idiopathic Ventricular Arrhythmias Originating From the Vicinity of the Communicating Vein of Cardiac Venous Systems at the Left Ventricular Summit. *Circ Arrhythm Electrophysiol*. 2018; Jan;11(1):e005386.
13. Kosiński A, Grzybiak M, Skwarek M, et al. Distribution of muscular bridges in the adult human heart. *Folia Morphologica*. 2004; 63(4), 491–498.
14. Kumagai K. Idiopathic ventricular arrhythmias arising from the left ventricular outflow tract: tips and tricks. *J Arrhythm*. 2014; 30(4):211–21.

15. Kuniewicz M, Baszko A, Ali D, et al. Left Ventricular Summit-Concept, Anatomical Structure and Clinical Significance. *Diagnostics (Basel)*. 2021; Aug 6;11(8):1423. doi: 10.3390/diagnostics11081423. PMID: 34441357; PMCID: PMC8393416.
16. Kuniewicz M, Budnicka K, Dusza M, et al. Gross anatomic relationship between the human left atrial appendage and the left ventricular summit region: implications for catheter ablation of ventricular arrhythmias originating from the left ventricular summit. *J Interv Card Electrophysiol*. 2022; Mar 9. doi: 10.1007/s10840-022-01172-6. Epub ahead of print. PMID: 35262858.
17. Kuniewicz M, Dobrzyński H, Karkowski G, et al. Septal summit: A narrow epicardial region above the left ventricular summit. Implications for electrophysiological procedures. *Kardiol Pol*. 2022; 80(7-8):849-852. doi: 10.33963/KP.a2022.0170. Epub 2022 Jul 19. PMID: 35851465.
18. Kuniewicz M, Krupiński M, Gosnell M, et al. Applicability of computed tomography preoperative assessment of the LAA in LV summit ablations. *J Interv Card Electrophysiol*. 2021; Aug;61(2):357-363. doi: 10.1007/s10840-020-00817-8. Epub 2020 Jul 14. PMID: 32666410; PMCID: PMC8324620.
19. Liao H, Wei W, Tanager KS, et al. Left ventricular summit arrhythmias with an abrupt V<sub>3</sub> transition: Anatomy of the aortic interleaflet triangle vantage point. *Heart Rhythm*. 2021; Jan;18(1):10-19. doi: 10.1016/j.hrthm.2020.07.021. Epub 2020 Jul 21. PMID: 32707175.
20. Mazur M, Holda M, Koziej M, et al. Morphology of tributaries of coronary sinus in humans. *Folia Medica Cracoviensia*. 2015; 55(2):5-13
21. McAlpine WA. *Heart and Coronary Arteries*. New York, NY: Springer-Verlag, 1975;
22. Obel OA, Avila A, Neuzil P, et al. Ablation of Left Ventricular Epicardial Outflow Tract Tachycardia from the Distal Great Cardiac Vein. *Journal of the American College of Cardiology*. 2006; 48 (9), 6–10.
23. PejkoVIC B, Bogdanovic D. The great cardiac vein. *Surg Radiol Anat*. 1992; 14(1):23-28.
24. Petersen HH, Chen X, Pietersen A, et al. Temperature-controlled irrigated tip radiofrequency catheter ablation: comparison of in vivo and in vitro lesion dimensions for standard catheter and irrigated tip catheter with minimal infusion rate. *J Cardiovasc Electrophysiol*. 1998; 9:409–14.
25. Sacher F, Roberts-Thomson K, Maury P, et al. Epicardial ventricular tachycardia ablation a multicenter safety study. *J Am Coll Cardiol* 2010; 55: 2366–2372.
26. Santangeli P, Marchlinski FE, Zado ES, et al. Percutaneous epicardial ablation of ventricular arrhythmias arising from the left ventricular summit: outcomes and electrocardiogram correlates of success. *Circ Arrhythm Electrophysiol* 2015;8: 337–343.
27. Whiteman S, Alimi Y, Carrasco M, et al. Anatomy of the cardiac chambers: A review of the left ventricle. *Translational Research in Anatomy*. 2021; Volume 23, June, 100095, <https://doi.org/10.1016/j.tria.2020.100095>
28. Słodowska K, Szczepanek E, Dudkiewicz D, et al. Morphology of the Left Atrial Appendage: Introduction of a New Simplified Shape-Based Classification System. *Heart Lung Circ*. 2021; Jul;30(7):1014-1022. doi: 10.1016/j.hlc.2020.12.006. Epub 2021 Feb 10. PMID: 33582020.
29. Topaz O, DiSciascio G, Vetrovec GW. Septal perforator arteries: From angiographic-morphologic characteristics to related revascularization options. *American Heart Journal*, 1992; 124 (3), 810–815.
30. von Lüdinghausen M. The venous drainage of the human myocardium. *Adv Anat Ebyrol Cell Biol* 2003; 168: I–VIII, 1–104
31. Wang Y, Di Biase L, Horton RP, et al. Left atrial appendage studied by computed tomography to help planning for appendage closure device placement. *J Cardiovasc Electrophysiol*. 2010; 21:973–982.
32. Whiteman S, Saker E, Courant V, et al. Translational Research in Anatomy An anatomical review of the left atrium. *Translational Research in Anatomy*. 2019; 17(September), 100052.
33. Yamada T, McElderry HT, Doppalapudi H, et al. Idiopathic ventricular arrhythmias originating from the left ventricular summit anatomic concepts relevant to ablation. *Circulation: Arrhythmia and Electrophysiology*. 2010; 3 (6), 616–623.

**Table 1** Morphometric characteristics of the LVS in cadaveric (n=80) and CT (n=48) samples

<b>Parameter [number form fig 1C]</b>	<b>Combined DATA</b>	<b>Cadaveric 80</b>	<b>Angio-CT 48</b>	<b>P-value</b>
LCA ostium bifurcation [mm] (min-max)	9.59 ± 4.14 (1.61–21.6)	9.02 ± 4.04 (1.61–21.6)	10.54 ± 4.18 (3–21)	<b>P = 0.05</b>
LAD bifurcation – SP [mm] (min-max)	18.92 ± 5.19 (7.25–33.08)	18.2 ± 5.55 (7.25–33.08)	20.06 ± 4.47 (10–28)	<b>P = 0.05</b>
angle of LCA bifurcation in degrees [°] (min-max)	85.46 ± 15.94 (48–125)	87.41 ± 13.61 (55–124)	82.21± 18.91 (48–125)	P = 0.09
LVS from formula [mm <sup>2</sup> ] (min-max)	287.38 ±144.95 (33.69–792.2)	270.46± 160.21 (33.69–792.2)	291.58 ± 115.5 (91.58 – 556.04)	P = 0.44
LVS superior aspect [mm <sup>2</sup> ] (min-max)	145.62 ± 84.35 (6.74–429.12)	152.92 ± 90.19 (6.74–429.12)	133.42 ± 72.89 (39.11–322.8)	P = 0.18
LVS inferior aspect [mm <sup>2</sup> ] (min-max)	121.69 ± 94.38 (8.96–431.13) (n = 13 [10.9% with no inferior aspect)	127.07 ± 106.98 (19.29–431.13) (n = 6 [7.5%] with no inferior aspect)	112.01 ± 65.72 (8.96–253.78) (n = 7 [14.6%] with no inferior aspect)	P = 0.35  P = 0.20
LVS distribution – superior to inferior relation [%]*	Superior > Inferior 59/115 [50.2%] Superior < Inferior 34/115 [26.6%] Superior = Inferior 22/115 [17.2%]	Superior > Inferior 39/74 [52.7%] Superior < Inferior 20/74 [27%] Superior = Inferior 15/74 [20.3%]	Superior > Inferior 20/41 [48.8%] Superior < Inferior 14/41 [34.1%] Superior = Inferior 7/41 [17.1%]	P = 0.69  P = 0.43  P = 0.68
Coronary vessels trespassing through LVS Parity of distribution. [n] – number of coronary branches**	RI [30] Dx1 [58] Dx2 [9] Mg1 [53] Mg2 [3] LAD>Cx 32/107 [29.9%] LAD<Cx 35/107 [32.7%] LAD=Cx 40/107 [37.4%]	RI [16] Dx1 [44] Dx2 [6] Mg1 [33] Mg2 [3] LAD>Cx 24/71 [33.8%] LAD<Cx 22/71 [31%] LAD=Cx 25/71 [35.2%]	RI [14] Dx1 [14] Dx2 [3] Mg1 [20] Mg2 [0] LAD>Cx 8/36 [22.2%] LAD<Cx 13/36 [36.1%] LAD=Cx 15/36 [41.7%]	P = 0.23  P = <b>0.03</b>  P = 0.96  P = 0.22  P = 0.59  P = 0.51
Blank LVS***	N = 21/128 16.4%	N = 9/80 11.25%	N = 12/48 25%	P = 0.04
Type of LAA overlapping LVS	C: 44 (33.4%) CW: 41 (32%)	C: 28 (35%) CW:23 (28.7%)	C: 16 (33.3%) CW: 18 (47.5%)	P = 0.85  P = 0.3



	AH: 43 (33.6%)	AH: 29 (26.3%)	AH: 14 (29.2%)	P = 0.41
LVS to LAA distance [mm] (min-max)	5.45 ± 2.51 (1.5–12.2)	6.3 ± 2.55 (2.8–12.2)	5.14 ± 2.47 (1.5–10)	P = 0.04

\*from evaluation of the LVS, pattern samples without inferior area have been excluded.

\*\*from evaluation of the LVS pattern samples without additional coronary branches have been excluded; \*\*\*without coronary vessels; AH — arrowhead, C — cauliflower, CW — chickenwing, Cx — circumflex branch, Dx — diagonal branch, Mg — marginal branch, LAA — left atrial appendage, LCA — left coronary artery, LAD — left anterior descending, LVS — left ventricular summit, RI — ramus intermedius

**Table 2.** Morphometric characteristics of the LVS in female (n=40) and male (n=88) samples

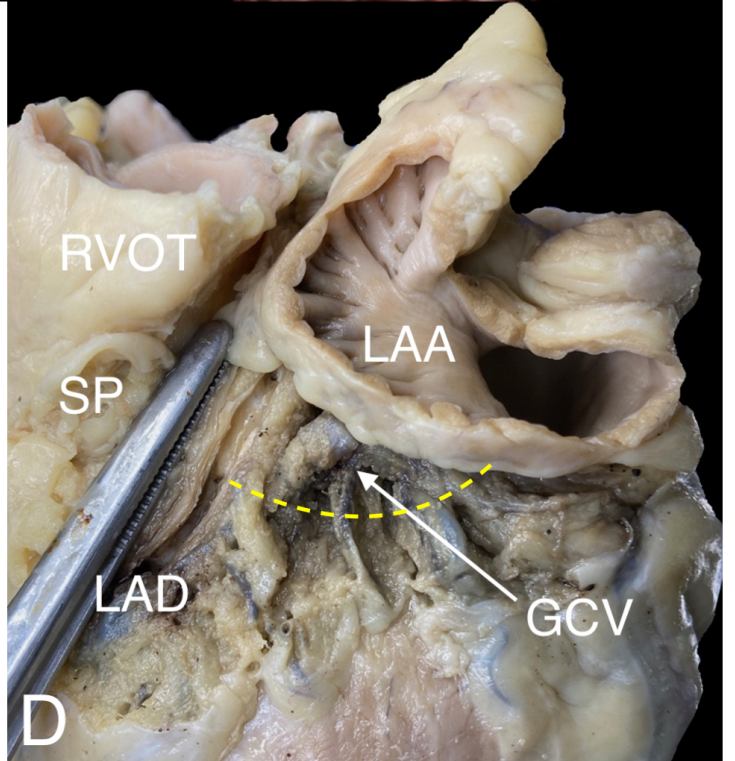
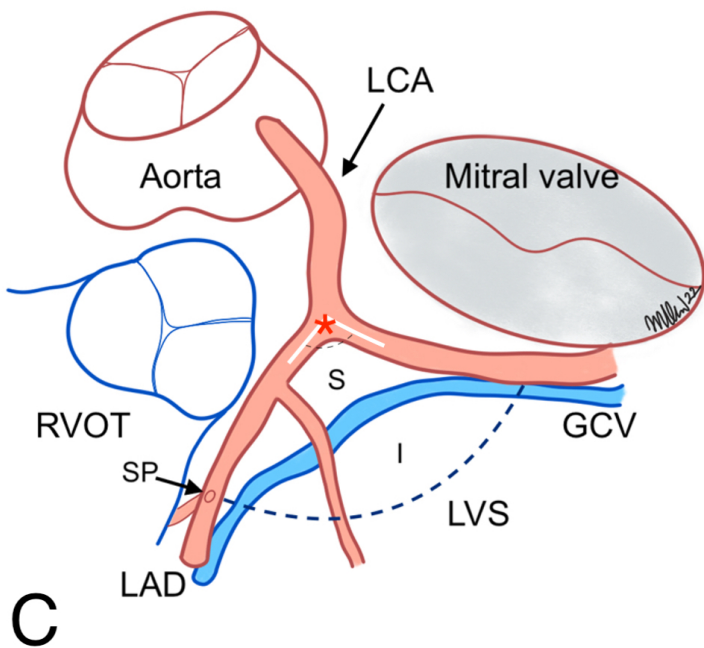
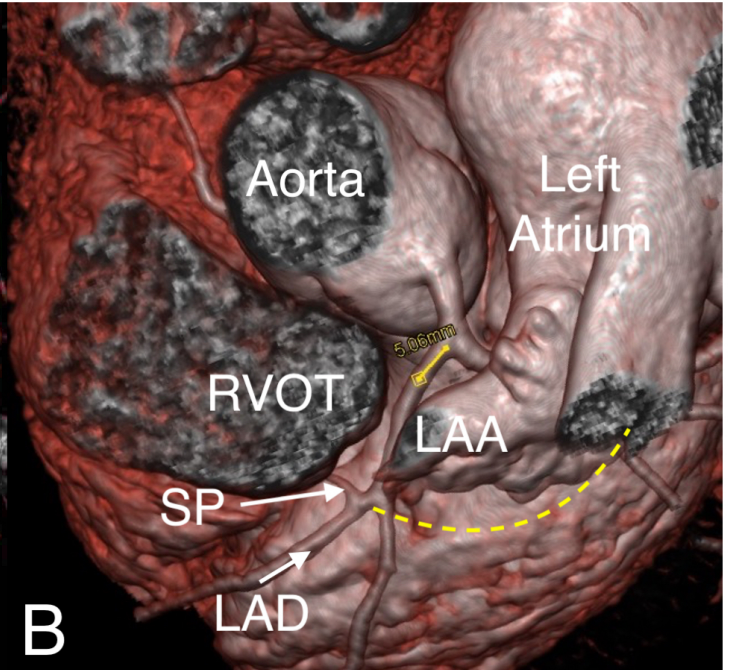
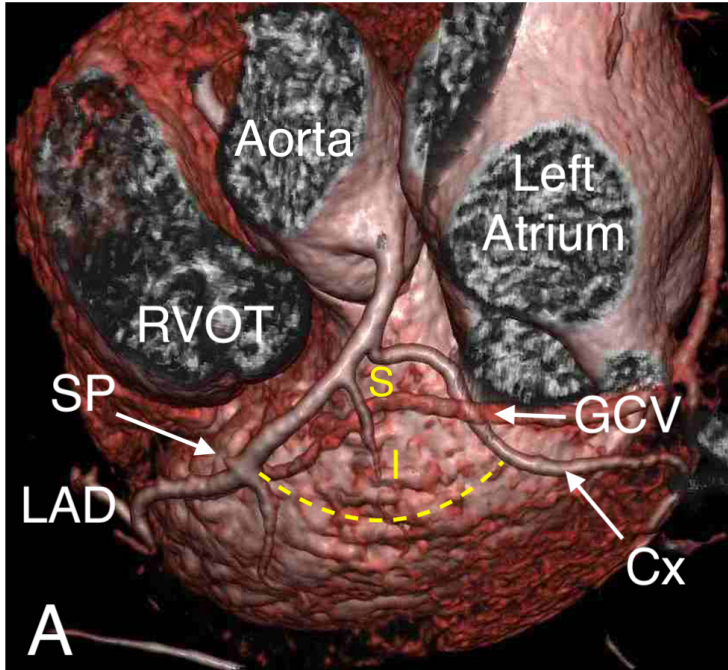
Parameter	Combined DATA	Female n-40	Male n-88	p-value
LVS from formula [mm <sup>2</sup> ] (min-max)	287.38 ± 144.95	244.71 ± 119.92	293.68 ± 152.3	P = 0.05
LVS superior aspect [mm <sup>2</sup> ] (min -max)	145.62 ± 84.35	127.8 ± 67.16	153.71 ± 89.78	P = 0.07
LVS inferior aspect [mm <sup>2</sup> ] (min -max)	121.69 ± 94.38 (n = 13 [10.9% with no inferior aspect])	81.58 ± 55.61 (n = 6 [7.5% with no inferior aspect])	138.53 ± 101.57 (n = 7 [14.6% with no inferior aspect])	P < 0.01 P = 0.3
LVS distribution – superior to inferior relation [%]*	Superior > Inferior 59/115 [50.2%] Superior < Inferior 34/115 [26.6%] Superior = Inferior 22/115 [17.2%]	Superior > Inferior 20/34 [58.8%] Superior < Inferior 7/34 [20.6%] Superior = Inferior 7/34 [20.6%]	Superior > Inferior 39/81 [48.2%] Superior < Inferior 27/81 [33.3%] Superior = Inferior 15/81 [18.5%]	P = 0.3 P = 0.17 P = 0.8
Blank LVS**	N = 21/128 16.4%	N = 11/40 27.5%	N = 10/88 11.4%	P = 0.02
LVS to LAA distance [mm]	5.45 ± 2.51	5.92 ± 2.6	5.11 ± 2.04	P = 0.05

\*from evaluation of the LVS pattern samples without inferior area has been excluded; \*\* without coronary vessels abbreviations; LAD — left anterior descending, LCA — left coronary artery, LVS — left ventricular summit

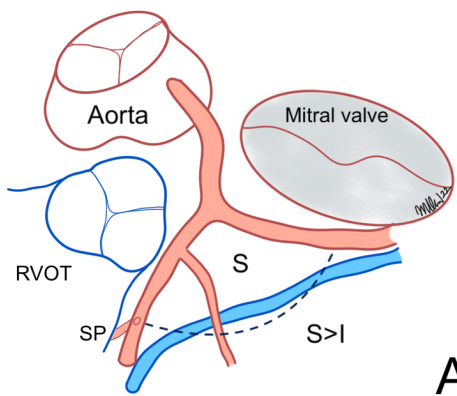
**Figure 1.** Left ventricular summit — views from the lateral and superior aspects. **A.** Photographs of the CT rendered image showing the LVS region without overlapping LAA; **B.** — rendered CT image of the LVS region covered by LAA. White asterisk —, red asterisks — septal summit; **C.** Schematic picture of presented structures; red asterisks indicate the point of LCA bifurcation with arms of the angle. S — superior area of the LVS, I — inferior area; **D.** Cadaveric heart with LVS region covered by an open LAA. The yellow/blue dotted line delineates the inferior border of the LVS; CT — computed tomography, Cx — circumflex artery, GCV — great cardiac vein, LAA — left atrial appendage, LAD — left anterior descending artery, LCA — left coronary artery, RVOT — right ventricle outflow tract, SP — septal perforator.

**Figure 2.** LVS schematic and study variations figures. **A.** Superior aspect dominance ( $S>I$ ), **B.** Equipoise between superior and inferior aspect ( $S=I$ ), **C.** Inferior aspect dominance ( $S<I$ ); **D.** E cadaveric hearts studies complementary to A and B figure and F — angio-CT rendered image with compliance to C figure; CT — computed tomography, GCV — great cardiac vein; I — inferior area, LAA — left atrium appendage; LAD — left anterior descending artery, RVOT — right ventricular outflow tract, LVS — left ventricular summit, S — superior area, SP — septal perforator, Blue/Yellow dotted line — delineates the inferior border of the LVS.

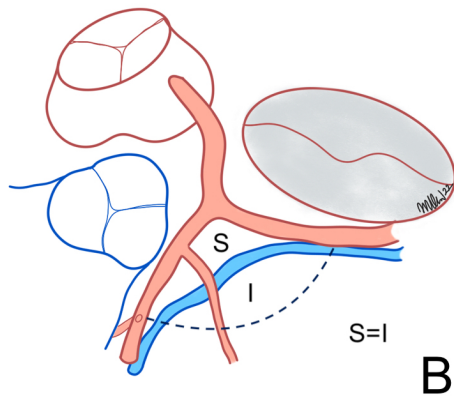
**Figure 3.** **A.** Angio-CT rendered image with suggested approach to the certain LVS regions, follow the description in the text. **B.** Cut through the LVS from R-L interleaflet trigon through the LVS; GCV — great cardiac vein, LAA — left atrium appendage, LAD — left anterior descending artery, LCC — aortic left coronary cusp; PT — pulmonary trunk; R-L ILT — right-left interleaflet trigon; RVOT — right ventricular outflow tract, LVS — left ventricular summit.



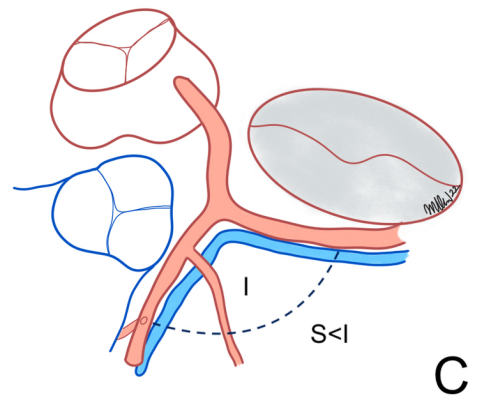




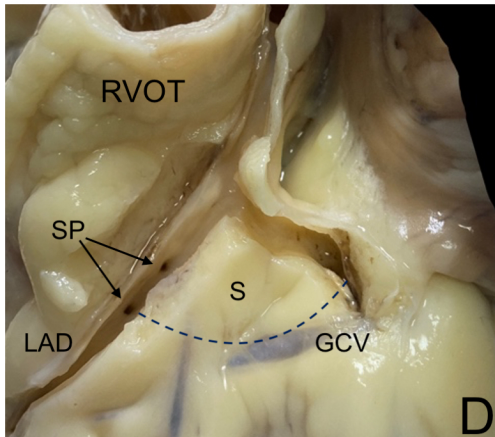
**A**



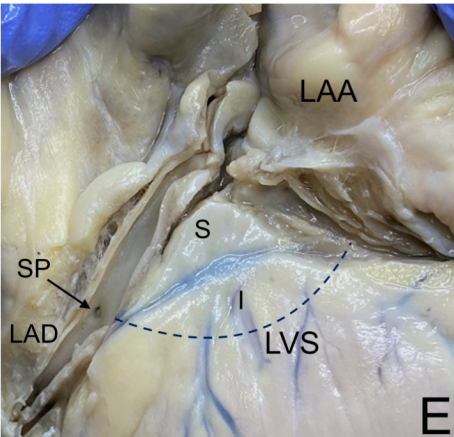
**B**



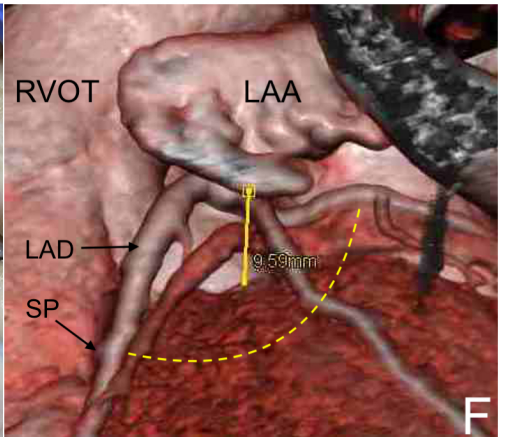
**C**



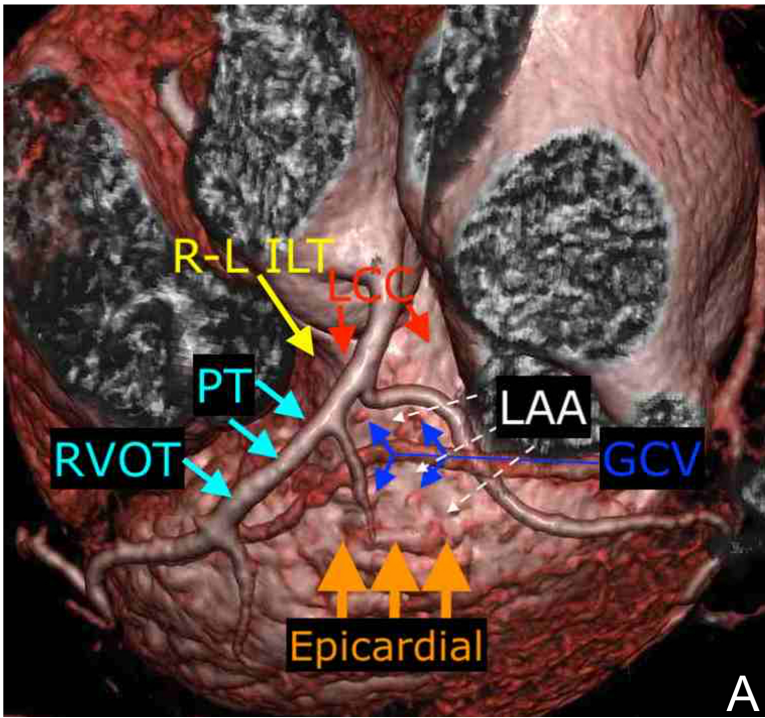
**D**



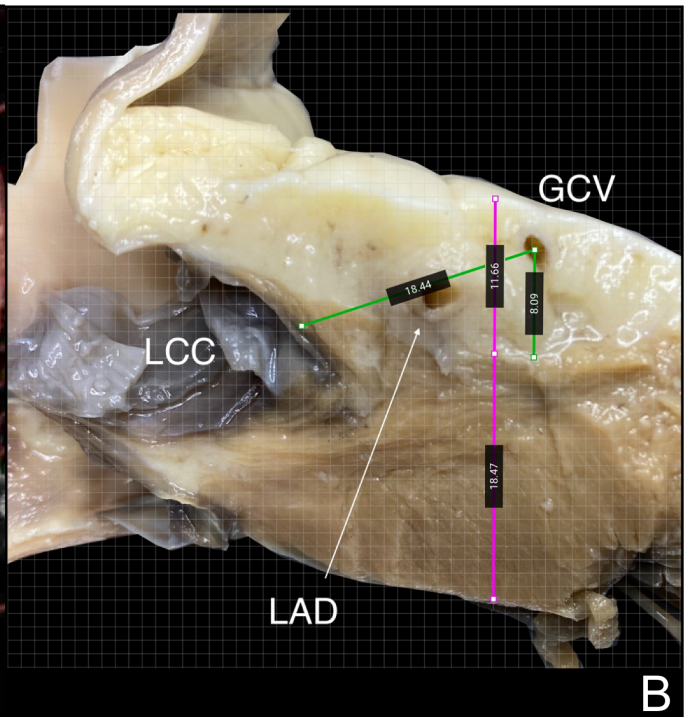
**E**



**F**



A



B